
Magnetorheological Finishing of Chemical-Vapor-Deposited Zinc Sulfide via Chemically and Mechanically Modified Fluids

Introduction

The importance of surface finishing an optical element is essential for preventing light scattering and absorption and improving imaging performance. In polycrystalline, chemical-vapor-deposited (CVD) materials, such as zinc sulfide (ZnS) and zinc selenide (ZnSe), surface finishing can be more challenging than in amorphous materials, such as glass.^{1–3} The presence of many crystallites (grains) within the polycrystalline, along with the crystal growth technique; i.e., CVD, gives rise to two post-polishing effects referred to as “orange peel” and “alligator skin.” In the orange peel effect, the finished surface has a visible pitted and uneven surface texture that reminds one of an orange peel. This effect occurs when the material is subjected to variations in the stalk removal rate during polishing among the different crystallites because of anisotropy in physical properties.^{4,5} Furthermore, grain boundaries are subjected to even higher material removal (than the grains) because of a higher concentration of microstructural defects, such as vacancies.⁵ Namba *et al.*⁴ showed that when the mechanical force (abrasive concentration) and the chemical force (slurry pH) are balanced during ultrafine finishing, one can overcome the inherent crystallite anisotropy and obtain a relatively uniform removal rate among different crystallite orientations (100, 110, and 111) of MnZn ferrite. When polishing polycrystalline MnZn ferrite with the balanced slurry, a smoother surface finish was observed. Similarly, Gavarischuk *et al.*⁵ investigated the chemical erosion of several acids on polycrystalline, CVD ZnSe substrates. They found that when the chemical erosion is well matched with the applied normal force (mechanical driving force) during conventional planetary polishing, a better surface finish is the result.

In the alligator skin effect, which is typical for CVD-grown materials, multiple millimeter-sized pebblelike structures appear on the finished surface.^{3,6–9} This happens when gas-phase particles that are formed in the furnace space land on the grown surface or mandrel during the CVD process. It appears that each particle becomes a nucleation site wherein crystallites grow radially, away from it, forming a hillock structure.⁶ Hillocks grow larger with deposition and manifest on the top

surface as pebbles. Zscheckel *et al.*¹⁰ used electron backscatter diffraction (EBSD) to show that the conelike structure within CVD ZnS is practically a collection of multiple crystallites with similar crystallographic orientation—in other words, a collection of textured grains. Each hillock structure is composed of many grains that differ slightly in crystallographic orientation from one another but differ significantly from grains of neighboring hillocks. Based on these findings, we expect that CVD materials are subjected to additional anisotropy in the pebbles regime. It is natural to hypothesize that different pebbles vary in their physical properties as a result of such anisotropy. This leads to variations in the material-removal rate (MRR) during polishing, which are later identified as surface artifacts.

Kozhinova *et al.*⁹ studied the magnetorheological (MR) fluid composition and conditions that reduce emergence of pebbles on a few substrates of polycrystalline, CVD ZnS during magnetorheological finishing (MRF). They changed the MR fluid composition [abrasive type, carbonyl iron (CI) type, and fluid pH] and followed the pebbles' emergence level. They succeeded in reducing pebble emergence when using the MR fluid with soft CI and acidic pH. Based on Kozhinova's work, Hallock *et al.*¹¹ showed a reduction in surface texture on polycrystalline ZnS and polycrystalline ZnSe surfaces when using altered MR fluid. In both cases, however, the use of acidic MR fluid gave rise to accelerated corrosion of the carbonyl iron particles, preventing any far-reaching application.

The MRF of CVD ZnS without surface artifact formation is very advantageous. Chemical-vapor-deposited ZnS is an important infrared (IR) material for the production of aerodynamic domes and windows.² Integrating a high-precision polishing technique that is able to fabricate complex and free-form optics (such as MRF) from this material is of great importance.

Our goal is to reduce surface features in the MRF of CVD ZnS while also greatly delaying any corrosion of CI particles. Here we investigate the anisotropy of CVD ZnS by using single-crystal orientations of ZnS. We study the individual contribution of mechanical (microhardness) and chemical

(erosion-rate) effects to material removal during polishing on four single-crystal planes: (100), (110), (111), and (311). We further investigate anisotropy of CVD ZnS during MR finishing by using three chemically and mechanically modified MR fluids at pH 6, 5, and 4. The ideal conditions in which a uniform MRR is obtained for all crystallographic orientations are identified. We demonstrate that applying these conditions on the polycrystalline, CVD ZnS material indeed reduces surface texture and surface artifacts during MR finishing.

Experimental

1. Single-Crystal and Polycrystalline CVD ZnS Substrates

Four single-crystal orientations of ZnS—(100), (110), (111), and (311)—were purchased from SurfaceNet.¹² Three unfinished blanks from each orientation (a total of 12 substrates) were cut from a large single-crystal ingot of cubic phase ZnS that was grown using the Bridgman–Stockbarger technique. Each single-crystal blank measured ~20 mm in diameter and ~1 mm thick. The cutting angle was calculated and later verified via the Laue diffraction. After delivery, the different crystallographic orientations were further tested and evaluated using Laue diffraction and x-ray diffraction texture analysis.

A polycrystalline CVD ZnS blank, measuring ~40 mm in diameter and 5 mm thick, was purchased from Rohm and Haas.¹³ All single-crystal and polycrystalline CVD ZnS substrates were polished in-house with diamond abrasives on pitch (as described in Ref. 9) to a peak-to-valley (p–v) flatness of 1 to 2λ , an areal roughness of less than 40-nm p–v, and a root mean square (rms) of less than 3 nm.

2. Tests for Evaluating Anisotropy in Polycrystalline CVD ZnS

a. Microhardness test. Microhardness measurements were performed using a diamond Vickers indenter on a TUKON 300BM microhardness tester. The testing load was 100 g for the single-crystal substrates and 200 g for the polycrystalline, CVD ZnS substrate. The samples were randomly selected and tested. A total of three identical indentations were placed on each part. We compared our experimental findings for the (100), (110), and (111) orientations with experimental data published

by Westbrook *et al.*¹⁴ and theoretical hardness values published by Li *et al.*¹⁵ We found no data in the literature for the (311) orientation; therefore, we followed the method described in Li *et al.*¹⁵ to calculate the theoretical microhardness of the (311) orientation.

b. Chemical reactivity test. The pre-polished substrates (single crystal and polycrystalline ZnS) were etched using an aggressive etching agent developed in our laboratory (and described in detail in Ref. 16). One drop (~0.02 ml) of etchant was applied inside a 1/8-in. hole that was punched on a commercial “blue painter’s tape” and taped on the part surface. Etching time was set at 4 min, resulting in a cylindrical “etching spot” with a relatively uniform depth. The etching depth (μm) was determined by averaging six lineout profiles across the center of the etched spot that were collected using a laser interferometer.¹⁷

c. Calculation of planar and bond densities. Calculations of planar density (PD) and bond density (BD) for each single-crystal plane (with Miller indices h , k , and l) were based on a cubic unit cell structure of ZnS (zinc blend or sphalerite). We defined planar density as the area of both zinc and sulfur atoms that were centered on the hkl plane divided by the area of the plane.¹⁸ We defined bond density, in a general form, as the number of Zn–S bonds across the hkl plane divided by the plane area (motivated by Ref. 19).

3. MR Fluids

The MR fluid composition used to prepare the low-pH polishing fluids is presented in Table 144.I. The magnetic particles made of zirconia-coated CI showed a high resistance to corrosion.²⁰ For better dispersion of these particles in an acidic, aqueous suspension, we used polyethylene-imine (PEI) as a dispersing agent (Sigma–Aldrich). This type of dispersant is common when using zirconia-based suspensions at a low-pH range since it shifts the isoelectric point (a pH at which the zeta potential of a suspension is ~0 mV) of such suspensions to the alkaline region;²¹ the same is true for the zirconia-coated-CI-based MR fluids (see App. B in Ref. 16). The initial pH of the

Table 144.I: Initial MR fluid composition before adjusting the pH.

Component	Density (g/cm ³)	Volume (mL)	Mass (g)	Volume (%)	Mass (%)
Zirconia-coated carbonyl iron (CI) powder	6.72	384.80	2583.93	38.60	80.67
Polyethylene-imine (PEI)	1.10	69.68	76.65	6.99	2.39
DI water	1.00	542.36	542.36	54.41	16.93
Total		996.84	3202.94	100.00	99.99

fluid after mixing the components of Table 144.I was 5.88 [all pH measurements are within the measuring device standard deviation of $\pm 1\%$ (± 0.01 units), unless indicated differently]. To modify the fluids pH, we used a few milliliters of an 8-M nitric acid solution (Sigma–Aldrich).

The off-line viscosity (η) of the MR fluids was measured using a Brookfield cone/plate Rheometer.²² At each pH, ~ 0.5 ml of fluid was extracted directly from the mixing vessel of the MRF machine and placed on the viscometer plate. The fluid was sheared for ~ 15 min before the viscosity as a function of shear rate (from 40 to 1000 1/s) was collected. Each measurement was repeated three times.

4. MRF Spotting Experiment

The MRF machine used in this work is a research platform referred to as the “spot-taking machine” (STM).²³ This type of machine has similar features to a conventional MRF machine. It has a peristaltic pump that circulates the MR fluid; a mixing vessel where the MR fluid is being continuously stirred and mixed; and a nozzle that ejects the MR fluid onto a rotating wheel located in a magnetic field. The MR fluid for polishing is water based and contains more than 80 wt% of micron-sized carbonyl iron (CI) particles. Because of the CI particles within the MR fluid, once the fluid is ejected on the wheel, it changes its form into a stiff ribbon that makes contact with and polishes an optical substrate. The main difference between our STM and a conventional MRF machine is the inability of the optical substrate to rotate or move in the x and y directions on the STM. This results in a single spot on the surface that has fine grooves in the direction of the wheel rotation.

The single-crystal planes were spotted for 1 min, while the polycrystalline was spotted for 10 min. For the single-crystal substrates, our interest was the relative removal rate among the different orientations; consequently, a short spotting time was sufficient. For the polycrystalline, we were interested in exposing the pebbles' structure; therefore, we had to remove at least $0.5 \mu\text{m}$ of material from the initial pre-polished surface, as explained by Kozhinova *et al.*⁹

The MR fluid in Table 144.I was loaded onto the STM and its pH increased slightly to 6.00 ± 0.01 . One spot was taken on each substrate (single-crystal and polycrystalline, CVD), giving a total of three identical spots for each single-crystal orientation and one spot for the polycrystalline, CVD substrate. The pH was lowered from 6.00 to a pH of 5.12 using ~ 4 ml of 8-M nitric acid. Each substrate was spotted once. The pH throughout this portion of the experiment (~ 70 min) was 5.11 ± 0.07 . The fluid

pH was further decreased using ~ 5 ml of 8-M nitric acid until it reached 4.19. During this stage of the spotting experiment, additional 8-M nitric acid was continuously added to the STM mixing vessel to maintain the pH level at ~ 4.20 . Throughout this portion of the experiment (~ 70 min), the pH was 4.25 ± 0.12 . The machine settings were a ribbon height of 1.4 to 1.6 mm, a penetration depth of 0.2 mm, a wheel speed of 200 to 250 rpm, a pump speed of 110 rpm, and an electric current of 15 A. When the experiment was finished, each substrate (single-crystal and polycrystalline, CVD) had three spots on it, one for each pH (see Fig. 144.17). For simplicity, from here on, we will refer to fluid pH values of 4.25 and 5.11, as pH 4 and 5, respectively.

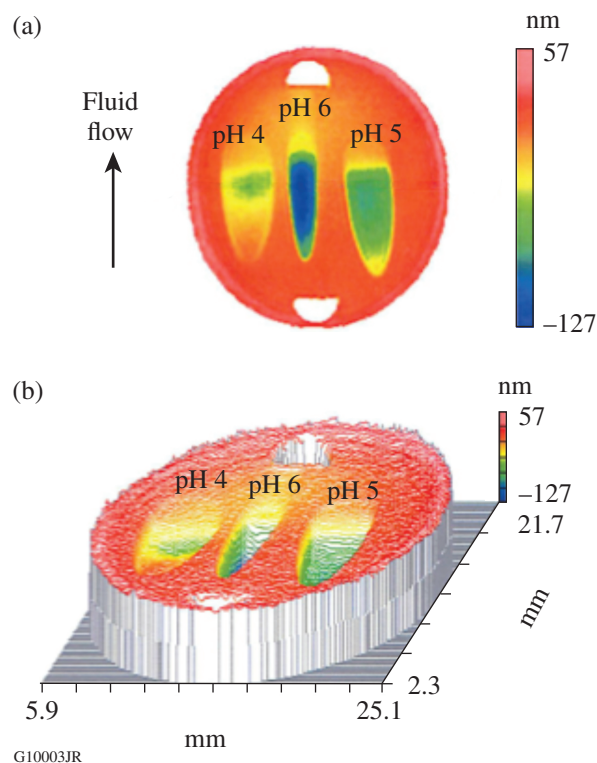


Figure 144.17

(a) A two-dimensional and (b) three-dimensional laser interferometer image of a single-crystal substrate with (100) orientation. The spots were taken with our zirconia-coated–CI MR fluids at pH levels of 4, 5, and 6.

5. Metrology

Material removal rates for chemical erosion and MRF spots were obtained with a Zygo Mark IV laser interferometer¹⁷ by subtracting the original surface from the etched or spotted area, respectively. Surface microroughness values were obtained with a Zygo NewView 100 white-light interferometer equipped with a $20\times$ Mirau objective.²⁴ For spots taken on the single-crystal substrates, areal (rms) and p–v values are given as an average of 15 measurements (five measurements

on each substrate, three substrates from each orientation) collected within the depth of deepest penetration (ddp) for each spot. In addition, 20 lineout profiles were collected from one areal measurement at the ddp for each spot (a total of 60 for one orientation) in the direction of the MR fluid flow. (This action minimized the influence of the MR ribbon grooves on the roughness data, which resulted from having the part stationary and not rotating.) For the polycrystalline, CVD ZnS part, four areal rms and p-v measurements were taken at the ddp of each spot. For each areal measurement, five lineout profiles were collected. Overall, 20 lineout profiles were averaged for each spot at a given pH.

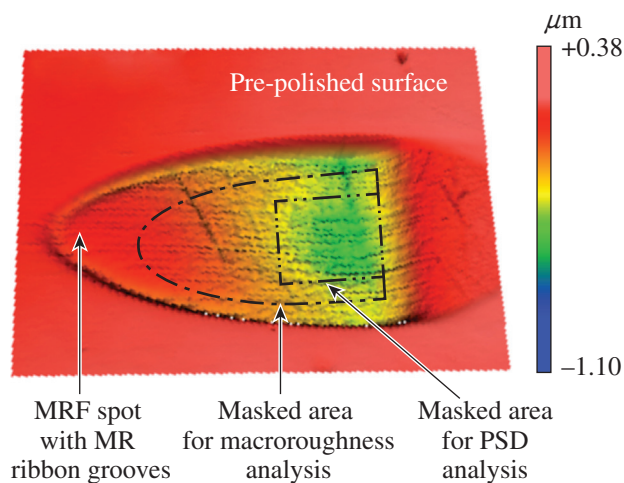
Surface texture and pebbles' emergence inside the spots taken on the polycrystalline, CVD ZnS substrate were obtained using a Zygo NewView 5000 white-light interferometer equipped with a 1× Mirau objective and a 0.8× zoom.²⁵ The use of low magnification was more suitable for observing and evaluating submillimeter features, such as pebbles. To analyze the spotted area, we masked the spots along their inner edge. From the remaining masked surface, a cylinder shape was removed. For the remaining masked area, the areal rms roughness was

recorded along with ten lineout profiles drawn in the direction of the MRF ribbon grooves. In addition, a power spectral density (PSD) analysis was performed in the direction of fluid flow by using the “average X PSD” function in the accompanying software MetroPro. For this analysis we masked a rectangular area (2 mm × 1 mm) around the ddp of each spot. Figure 144.18 shows the different masks used for roughness collection and PSD analysis. Both data analyses (rms roughness and PSD) provided us with information about the waviness of the spotted surfaces. Note that roughness measurements taken at low magnification have relatively low resolution; therefore, the data shown here better represent surface texture rather than surface microroughness unless a 20× Mirau objective is being used.

Results

1. Anisotropy in CVD ZnS from Single-Crystal Behavior

The Vickers microhardness values of the different crystallographic planes tested at a 100-g load and the polycrystalline CVD substrate tested at a 200-g load are presented in Table 144.II, along with experimental Vickers hardness data from Westbrook *et al.*¹⁴ and theoretical predictions of Vickers hardness data published by Li *et al.*¹⁵ Experimental results show



G10302JR

Figure 144.18

A 3-D white-light interferometer image (9 × 8 mm) of a pre-polished polycrystalline, CVD ZnS substrate with an MRF spot taken with our zirconia-coated-CI MR fluid at pH 4. The dashed-dotted lines designate the masked areas used to obtain roughness and power spectral density (PSD) data. Lateral grooves are caused by the stiff MR ribbon because the part does not rotate on the spot-taking machine (STM).

Table 144.II: Experimental and theoretical Vickers microhardness of single-crystal ZnS planes and CVD ZnS.

Source	Vickers microhardness H_V (GPa)				CVD ZnS	Relative to (100) plane
	(100)	(110)	(111)	(311)		
Our work (100 g)	1.89±0.03	1.71±0.04	2.93±0.04	2.17±0.12	1.94±0.05 (200 g)	1.00; 0.91; 1.55; 1.15
Westbrook <i>et al.</i> , ¹⁴ wet (50 g)	1.50	1.80	2.00	n/a	n/a	1.00; 1.20; 1.33; n/a
Westbrook <i>et al.</i> , ¹⁴ dry (50 g)	1.32	1.61	1.87	n/a	n/a	1.00; 1.22; 1.42; n/a
Li <i>et al.</i> ¹⁵	2.08	2.32	2.90	2.26*	n/a	1.00; 1.12; 1.39; 1.09

*Calculated using the method from Ref. 15.

that the degree of anisotropy among planes (100), (110), and (311) varied between 9% to 15%. Between the (100) plane and the (111) plane, there is a maximum difference in microhardness of 55%. Ranking the Vickers hardness of the planes from low to high shows that $H_V110 < H_V100 < H_V311 < H_V111$. When comparing our findings with Westbrook *et al.*¹⁴ and Li *et al.*,¹⁵ we see that our results are in fair agreement with the data published by Westbrook *et al.*,¹⁴ but they agree better with the theoretical predictions of Li *et al.*¹⁵ For all sources, the (111) plane is the one with the highest Vickers hardness value. The polycrystalline CVD ZnS has a Vickers hardness value of ~2 GPa, closer in value to that of the (100), (110), and (311) planes.

Chemical etching results for the different single-crystal planes and the polycrystalline, CVD ZnS substrate are presented in Table 144.III. These results show that planes (100) and (110) share similar chemical erosion rates (4% anisotropy) that were slightly lower than that for the (311) plane. Plane (111) had a significantly slower chemical erosion rate (~30%) than that for the other planes, implying that this plane is less chemically reactive.

Calculations of planar density and bond density are provided in Table 144.IV. The results indicate a high degree of anisotropy among the single-crystal planes. In all cases, plane (111) has the highest values of hardness, the lowest erosion rate, and the highest bond and planar densities.

2. MRF of Single Crystal with Modified MR Fluids

a. Viscosity and removal rate of MR fluids. Figure 144.19 presents the off-line viscosity versus shear rate for all fluids. Our modified MR fluids have flow characteristics that are similar to those of the conventional MR fluid (inset plot in Fig. 144.19). All fluids show a higher viscosity at low shear rates that decreases (but stays relatively viscous) with increasing shear rate. This is a classic behavior of an MR fluid with a Bingham plastic flow.²⁶ We found that the viscosity of the zirconia-coated-CI fluid was pH dependent, even though the particles' concentration was roughly the same (80 to 81 wt%) throughout the experiment. At an ~800-1/s shear rate that is present when the MR fluid is ejected out from the nozzle, the fluid's off-line viscosities are ~47, ~109, and ~194 cP for pH

Table 144.III: Chemical-etching rates of single-crystal ZnS planes and CVD ZnS.

	(100)	(110)	(111)	(311)	CVD ZnS	Relative to (100) plane
Nominal etch rate (nm/min)	13.29±1.26	13.83±0.59	9.29±0.49	15.29±0.83	14.5±0.6	1.00; 1.04; 0.70; 1.15

Table 144.IV: Planar and bond densities calculated for single-crystal ZnS planes.

	(100)	(110)	(111)	(311)	Relative to (100) plane
Planar density (atoms/nm ²)	0.79	0.56	0.91	0.45	1.00; 0.70; 1.15; 0.57
Bond density (bonds/nm ²)	13.67	14.50	39.45	24.71	1.00; 1.06; 2.89; 1.81

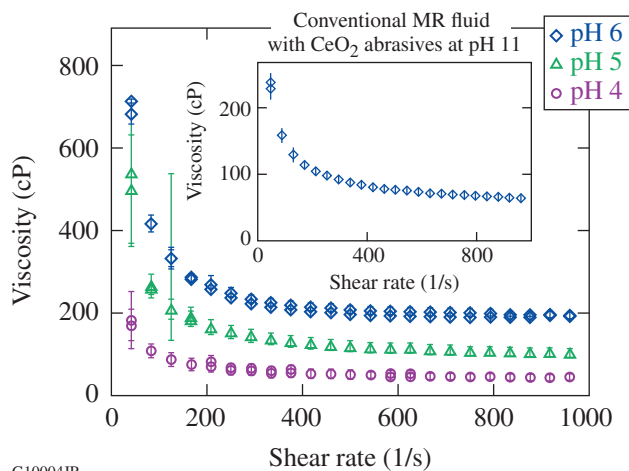


Figure 144.19 Plot of viscosity versus shear rate for zirconia-coated-CI MR fluids at pH 4 (circles), 5 (triangles), and 6 (diamonds). Viscosity is pH dependent and shows the lowest values at pH 4. The inset shows the viscosity pattern of a conventional MR fluid at pH 11 with uncoated CI and cerium oxide (CeO₂) abrasives.

G10004JR

4, 5, and 6, respectively. An ~50% increase in viscosity occurs for a pH increase of one unit.

The average peak removal rate and volumetric removal rates of the different fluids are given in Tables 144.V and 144.VI, respectively. For all single-crystal ZnS orientations, the peak removal rate decreases with decreasing fluid pH and viscosity. The average peak removal rate at pH 4 is about 50% lower than it is at pH 6, while keeping the magnetic particles' concentration constant within 1%. There is an apparent correlation among the fluid pH, viscosity, and removal rate. Higher pH causes higher viscosity, which leads to a higher removal rate. This confirms the expectation that the MRR being driven by shear stress increases as the viscosity (and shear stress) increases.

As for the volumetric removal rate, we see that at pH 6, results are similar to that of pH 5, but significantly (~50%) higher than pH 4.

Table 144.V: Average and standard deviations of peak removal rate ($\mu\text{m}/\text{min}$) for all orientations when polished with modified zirconia-coated-CI MR fluid at three pH levels.

Orientation	Average peak removal rate $\times 100$ ($\mu\text{m}/\text{min}$)		
	pH 4	pH 5	pH 6
(100)	6.00 ± 1.35	9.17 ± 0.57	12.93 ± 0.78
(110)	5.87 ± 0.93	8.93 ± 1.18	12.13 ± 1.16
(111)	5.37 ± 0.67	10.43 ± 1.53	14.03 ± 1.12
(311)	5.27 ± 0.31	8.13 ± 1.72	12.07 ± 0.57
Average of all orientations	5.63 ± 0.35	9.17 ± 0.95	12.79 ± 0.91

Table 144.VI: Average and standard deviations of volumetric removal rate ($\mu\text{m}/\text{min}$) for all four orientations when polished with modified zirconia-coated-CI MR fluid at three pH levels.

Orientation	Average volumetric removal rate $\times 10^5$ ($\mu\text{m}^3/\text{min}$)		
	pH 4	pH 5	pH 6
(100)	4.24 ± 0.61	7.58 ± 0.85	7.83 ± 0.97
(110)	4.39 ± 0.68	7.10 ± 1.62	7.16 ± 0.79
(111)	4.28 ± 0.13	8.66 ± 1.33	8.20 ± 0.42
(311)	4.04 ± 0.73	7.09 ± 1.44	7.52 ± 0.55
Average of all orientations	4.24 ± 0.15	7.61 ± 0.74	7.68 ± 0.44

When observing the relative peak and volumetric removal rates among the different single-crystal planes, the least anisotropy in removal rate is observed for the MR fluid at pH 4 and an off-line viscosity of ~47 cP. Supportive findings are given at the average line in Tables 144.V and 144.VI. The data show that the standard deviation of the average made from the individual averages of the single crystals is lowest when the samples are polished with a pH 4 MR fluid. This indicates that variations in removal rate among the single crystals polished with this fluid are minimal.

Figures 144.20(a) and 144.20(b) also present the data for the peak and volumetric removal rates, respectively. These results suggest that polishing the polycrystalline CVD ZnS material with this type of MR fluid (pH 4, off-line viscosity of ~47 cP) will provide a lower degree of pebbles and surface artifacts on the finished surface (as shown in **MRF of Polycrystalline CVD ZnS with Modified Fluids**, below).

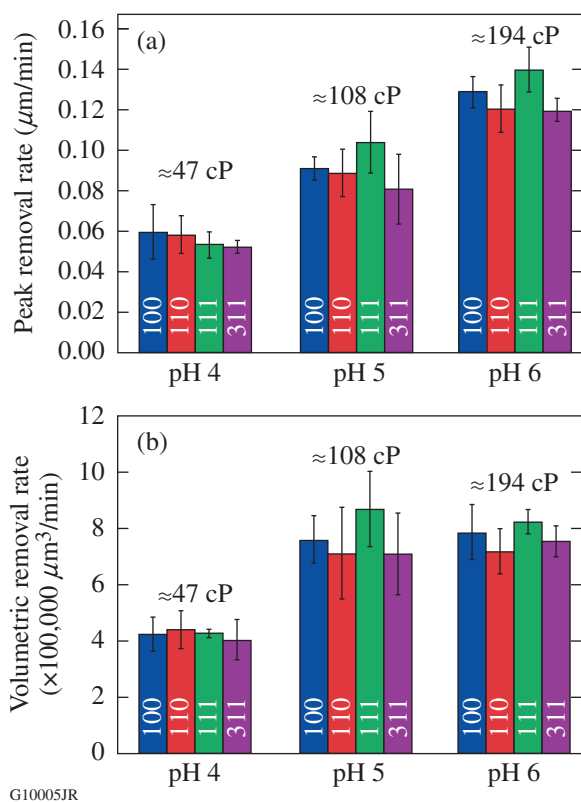


Figure 144.20 (a) Peak removal rate and (b) volumetric removal rate versus pH for all four orientations. The smallest degree of anisotropy in removal rate is observed at pH 4 and an off-line viscosity of 47 cP. Higher removal rates and anisotropies are observed at pH 5 and 6.

b. Surface roughness of MR-finished single-crystal ZnS. Surface roughness data at the ddp of the spotted single-crystal planes are summarized in Table 144.VII and Figs. 144.21(a) and 144.21(b). For each orientation we averaged the areal rms (nm) and lineout rms (nm) of three identical spots. For all planes, MRF with our altered fluids significantly roughened the pre-polished surface at all pH values. We noticed that the randomly distributed scratches on the surfaces, from the pre-polishing process, were enhanced during MRF with the altered fluids. The areal roughness increased with increasing fluid pH and viscosity. Roughness taken as lineouts shows about 50% smoother surfaces than the areal rms value. This is a result of avoiding the MRF grooves effect on the surface caused by the lack of part rotation. The least variation in the areal roughness among the different orientations is observed at pH 4 ($\eta \approx 47$ cP) [see Fig. 144.21(a)]. Lineout roughness as a function of pH for all orientations is given in Fig. 144.21(b). The results are similar

for all surfaces spotted at pH 4 and 5, with slightly higher values when spotted at pH 6. The least anisotropy is observed at pH 4 and an off-line viscosity of 47 cP for the areal measurements and at pH 4 and 5 at an off-line viscosity of ~ 47 and ~ 108 cP, respectively, for the lineout measurements.

3. MRF of Polycrystalline CVD ZnS with Modified Fluids

a. Pebbles' emergence on the surface. Figure 144.22 shows the PSD analysis for a CVD ZnS surface spotted with our zirconia-coated-CI MR fluids at pH 4, 5, and 6. Results show that surface texture and waviness are higher at pH 6, somewhat lower at pH 5, and significantly lower at pH 4. When summarizing the data as areal (a "D" shape of 2 mm \times 4 mm) rms and lineout profiles (3 to 4 mm long) in Table 144.VIII, we observed that macroroughness decreases as fluid pH and viscosity decrease. Moreover, standard deviation of data collected as lineout profiles at pH 4 and $\eta \approx 47$ cP

Table 144.VII: Areal and lineout rms surface roughnesses for the pre-polished and spotted single-crystal substrates.

	Pre-polished	pH 4		pH 5		pH 6	
Orientation	Areal rms (nm)	Areal rms (nm)	Line rms (nm)	Areal rms (nm)	Line rms (nm)	Areal rms (nm)	Line rms (nm)
100	1.71 \pm 0.22	9.73 \pm 4.39	4.38 \pm 1.40	10.54 \pm 2.83	4.34 \pm 2.01	16.15 \pm 3.65	8.08 \pm 4.92
110	1.73 \pm 0.35	8.21 \pm 3.25	3.55 \pm 1.00	12.64 \pm 5.68	3.78 \pm 1.47	19.03 \pm 4.53	6.07 \pm 1.89
111	1.69 \pm 0.36	8.27 \pm 2.32	4.24 \pm 1.05	14.35 \pm 3.14	4.19 \pm 1.19	22.89 \pm 8.76	5.24 \pm 2.23
311	2.84 \pm 1.97	8.71 \pm 3.23	3.39 \pm 1.29	13.22 \pm 5.63	3.25 \pm 0.90	18.14 \pm 5.82	4.13 \pm 1.25

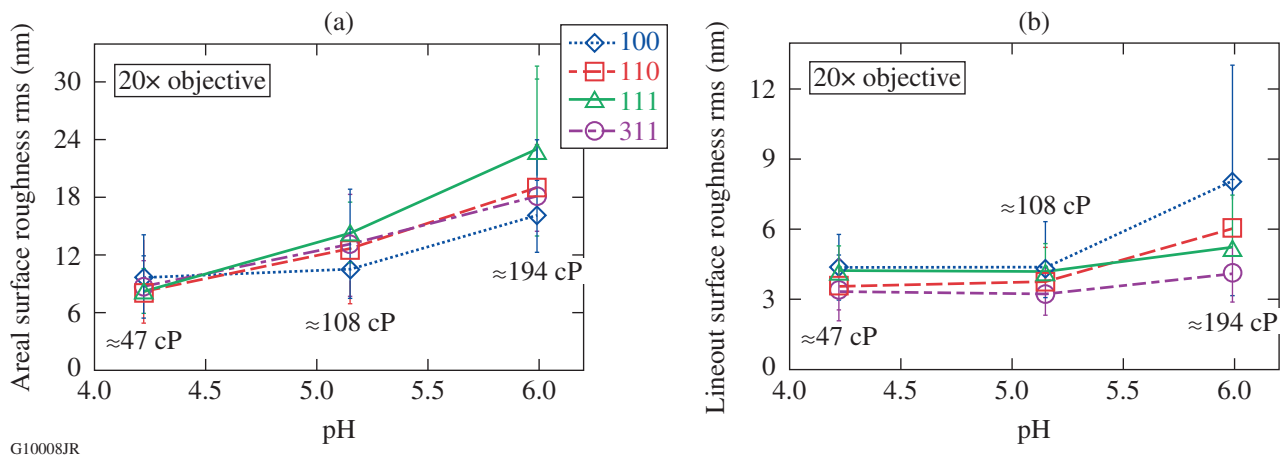


Figure 144.21 (a) Areal rms and (b) lineout rms versus pH for all four orientations. The least anisotropy is observed at pH 4 and an off-line viscosity of 47 cP for the areal measurements and at pH 4 and 5 at an off-line viscosity of 47 and 108 cP, respectively, for the lineout measurements.

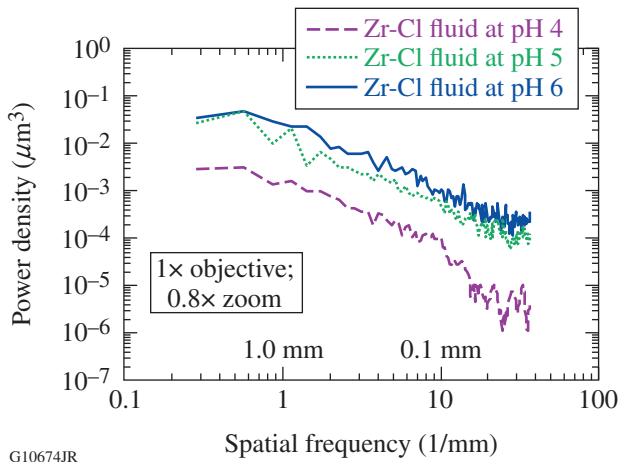


Figure 144.22 Average PSD along the *x* direction for our zirconia-coated-CI MR fluids at pH 4 (solid), pH 5 (dotted), and pH 6 (dashed).

is significantly lower than that of pH 5 and 6. We emphasize that roughness measurements were taken at a low resolution. At a scale length of 0.05 to 1 mm (a spatial frequency of 1 to 20 1/mm), these data better represent surface texture rather than surface microroughness. All three data analysis (PSD, areal, and lineout macroroughness) results show that the surface of polycrystalline CVS ZnS polished with MR fluid at pH 4 and $\eta \approx 47$ cP has the least degree of pebble features at the surface.

Table 144.VIII: Areal and lineout rms surface roughnesses collected from masked spots taken with zirconia-coated-CI MR fluids at pH 4, 5, and 6 on a pre-polished surface of CVD ZnS substrates from Rohm and Haas.

	pH 4	pH 5	pH 6
Areal rms (μm)	18	44	66
Lineout profiles rms (μm)	16.4±2	38.78±9	60±20

b. Surface microroughness. Figure 144.23 shows the surface microroughness at the ddp of the spotted polycrystalline CVD ZnS substrate at pH values of 4, 5, and 6. Similar to the single-crystal substrates, MRF with our altered fluids significantly roughened, as expected, the pre-polished surface at all pH values. Areal microroughness (rms) at pH 6 is similar to that at pH 5 and ~38% higher than that at pH 4. Roughness taken as lineouts (rms) shows a reduction in microroughness with reduced pH. Once again we see that polishing with MR fluid at pH 4 and $\eta \approx 47$ cP provides smoother surfaces among the three tested pH values.

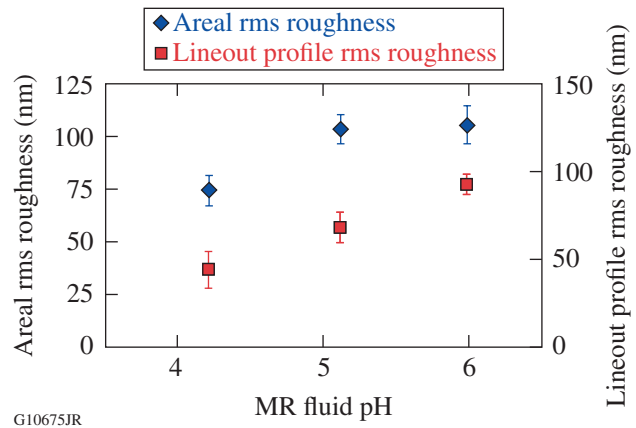


Figure 144.23 Microroughness (rms) versus fluid pH for zirconia-coated-CI MR fluids at pH 4, 5, and 6. The left vertical axis designates an average of four areal measurements taken at the ddp; the right vertical axis designates an average of 40 lineout profiles (ten lineouts per one areal measurement). All measurements were taken with a 20× objective.

Discussion

Differences in microhardness, chemical erosion, and planar and bond densities among all planes were observed, especially between the (111) orientation and the (110), (100), and (311) orientations. Plane (111) has the highest hardness, highest planar and bond densities, and the lowest chemical reactivity of all four planes. These findings of anisotropy in physical properties among the different single crystals are what lead us to believe that the polycrystalline material might be subjected to an uneven material removal during the MRF process, which results in high surface texture and roughness.

We extended our tests to check anisotropy in the MRR among the different crystallographic orientations during MRF. Again we found differences among the different orientations (note that, in this case, MRF includes both mechanical and chemical effects at the same time). We do see, however, that uniformity in material removal among the different planes is improved with a reduction in MR fluid pH and viscosity. Moreover, minimal variation in peak and volumetric removal rates among the different crystallographic orientations is observed when polishing with MR fluid at pH 4 and $\eta \approx 47$ cP. Further investigation of these results shows that when MR finishing the polycrystalline, CVD ZnS material with the pH 4 ($\eta \approx 47$ cP) MR fluid, the appearance of pebbles on the surface was minimized.

Among all three tested MR fluids, the low-pH, low-viscosity MR fluid seems to provide the ideal balance between mechanical

and chemical driving forces during MRF, helping to overcome the anisotropic nature of polycrystalline CVD ZnS. With that said, the use of low-pH and low-viscosity MR fluid also reduced dramatically the peak removal rate from $\sim 0.16 \mu\text{m}/\text{min}$ at pH 6 ($\eta \approx 194 \text{ cP}$) to $\sim 0.10 \mu\text{m}/\text{min}$, at pH 5 ($\eta \approx 108 \text{ cP}$), and to $\sim 0.06 \mu\text{m}/\text{min}$ at pH 4 ($\eta \approx 47 \text{ cP}$). It is known that an acid or a base can be used as a dispersing agent when added to an aqueous suspension since it increases the particles' zeta potential and shifts the suspension to a pH region far from its isoelectric point (IEP).²⁷ In our case, the fluid described in Table 144.I has an IEP at $\sim \text{pH } 10$ (Ref. 16); therefore, the lower the fluid pH, the less viscous it is. In addition, lower viscosity leads to lower contact shear stresses (where the strain value remains constant), confirming the previous result that the MRR is driven by shear contact stresses.²⁸

Lower viscosity of the fluid causes the MR fluid ribbon to expand to the sides under applied normal pressure from the workpiece's surface. Also, lower viscosity affects the spot's geometry. A supportive observation for this is given in Fig. 144.17—a Mark IV laser interferometer image of single-crystal plane (100) spotted with the three MR fluids at pH 6, 5, and 4. We clearly see the difference in the spots' dimensions. At pH 6 the spot is very narrow and deep caused by stiff and viscous ribbon; at pH 5 the spot is wider and shallower; and at pH 4 the spot is the widest and shallowest among the three. This was observed for all spotted single-crystal and polycrystalline substrates. By achieving the ideal balance between mechanical and chemical forces, we also produced a low MRR, making our MRF process slower.

The pre-polished surfaces of both single-crystal planes and polycrystalline CVD ZnS polished with our altered MR fluids were roughened at all pH values, as expected (because of the lack of polishing abrasive in our fluids). In particular, roughness increased with an increase in pH. Lineout profile roughness shows smoother surfaces (50%-smaller rms) than the areal value (as a result of avoiding the MRF grooves on the surface caused by lack of part rotation), but they are still relatively high for the single-crystal planes and even higher for the polycrystalline material. It seems that the zirconia present in the coating and as free particles in the MR fluid and the lack of polishing abrasives cause the relatively high surface roughness. Zirconia is not the kind of abrasive that is commonly used in the MR finishing industry. Commercial MR fluids usually contain nanodiamond, ceria, or alumina abrasives.²⁹ Further experiments with additional types of abrasives will

try to achieve higher removal values and smoother surface roughness, in addition to improving the surface texture that was observed here.

Conclusions

The physical basis for anisotropy of polycrystalline CVD ZnS was investigated using four single-crystal orientations. Microhardness and chemical etching results for the single-crystal ZnS planes identified variations among the planes and the (111) crystallographic orientation as the most-unique orientation. This can be explained by our theoretical calculations of planar and bond densities, which show the differences in the number of Zn and S atoms and Zn–S bonds between the different planes. During MRF, anisotropy in the MRR among the single-crystal planes was also observed. The difference among the four orientations could provide a scientific explanation for the surface-texture issues experienced during MRF of CVD ZnS.

Changing the zirconia-coated-CI MR fluid pH affects the fluid viscosity and the overall material-removal rate. Moreover, variations in the MRR between the single crystals are minimized when polishing with fluid at a pH ~ 4.22 and an off-line viscosity of $\sim 47 \text{ cP}$. Roughness was also minimized with this type of fluid at pH 4, although overall it is relatively high. When the polycrystalline, CVD ZnS surface was MR finished with pH 4, 5, and 6 MR fluids, we saw a reduction in surface texture and roughness as the fluid pH and viscosity went down. The least degree of surface texture and roughness was obtained with a pH 4 MR fluid as a result of relatively uniform MRR among the single-crystal planes under these conditions.

It is clear from our results that there is an optimal balance between mechanical (crystallography, strain rate, viscosity) and chemical (pH) effects in the MRR of ZnS. A relatively low pH minimizes variations in the MRR among different crystallographic orientations. We have also shown that the CI corrosion can be significantly reduced by using our zirconia-coated particles at such a low pH.

ACKNOWLEDGMENT

This material is based upon work supported by the Department of Energy National Nuclear Security Administration under Award Number DE-NA0001944, the University of Rochester, and the New York State Energy Research and Development Authority. The support of DOE does not constitute an endorsement by DOE of the views expressed in this article. This work is synergistic with the NSF I/UCRC Center for Freedom Optics (IIP-1338877 and IIP-1338898).

REFERENCES

1. L. L. Gregg, A. E. Marino, J. C. Hayes, and S. D. Jacobs, in *Optical Manufacturing and Testing V*, edited by H. P. Stahl (SPIE, Bellingham, WA, 2004), Vol. 5180, pp. 47–54.
2. D. C. Harris, *Materials for Infrared Windows and Domes: Properties and Performance, Tutorial Texts in Optical Engineering* (SPIE Optical Engineering Press, Bellingham, WA, 1999), p. 145.
3. J. S. Goela and R. L. Taylor, *J. Mater. Sci.* **23**, 4331 (1988).
4. Y. Namba and H. Tsuwa, *CIRP Ann.* **28**, 425 (1979).
5. E. M. Gavrishchuk *et al.*, *Inorg. Mater.* **43**, 579 (2007).
6. K. L. Lewis *et al.*, in *Proceedings of the Ninth International Conference on Chemical Vapor Deposition 1984*, edited by Mc. D. Robinson *et al.* (Electrochemical Society, Pennington, NJ, 1984), pp. 530–545.
7. J. S. McCloy, “Properties and Processing of Chemical Vapor Deposited Zinc Sulfide,” Ph.D. thesis, University of Arizona, 2008.
8. W. F. Adler, J. C. Botke, and T. W. James, Wright-Patterson Air Force Base, Ohio, Technical Report AFML-TR-79-4151 (October 1979).
9. I. A. Kozhinova, H. J. Romanofsky, A. Maltsev, S. D. Jacobs, W. I. Kordonski, and S. R. Gorodkin, *Appl. Opt.* **44**, 4671 (2005).
10. T. Zscheckel, W. Wisniewski, and C. Rüssel, *Adv. Funct. Mater.* **22**, 4969 (2012).
11. B. Hallock *et al.*, in *Frontiers in Optics 2008/Laser Science XXIV/ Plasmonics and Metamaterials/Optical Fabrication and Testing*, OSA Technical Digest (CD) (Optical Society of America, Washington, DC, 2008), Paper OThB2.
12. SurfaceNet GmbH, Landersumer Weg 40, D-48431 Rheine, Germany.
13. Rohm and Haas Company, a subsidiary of Dow Chemical Company, Philadelphia, PA 19106-2399.
14. J. H. Westbrook and P. J. Jorgensen, *Am. Mineral.* **53**, 1899 (1968).
15. K. Li, P. Yang, and D. Xue, *Acta Mater.* **60**, 35 (2012).
16. S. Salzman, H. J. Romanofsky, Y. I. Clara, L. J. Giannechini, G. West, J. C. Lambropoulos, and S. D. Jacobs, in *Optifab 2013*, edited by J. L. Bentley and M. Pfaff (SPIE, Bellingham, WA, 2013), Vol. 8884, Paper 888407.
17. Zygo Mark IVxp™, Zygo Corporation, Middlefield, CT 06455.
18. I. P. D. Sadoway, *3.091SC Introduction to Solid State Chemistry*, MIT Online Course, Materials Science and Engineering, Massachusetts Institute of Technology, Cambridge, MA (Fall 2010).
19. F. Gao *et al.*, *Phys. Rev. Lett.* **91**, 015502 (2003).
20. R. Shen, S. N. Shafirir, C. Miao, M. Wang, J. C. Lambropoulos, S. D. Jacobs, and H. Yang, *J. Colloid Interface Sci.* **342**, 49 (2010).
21. T. Fengjiu *et al.*, *Ceram. Int.* **26**, 93 (2000).
22. Brookfield DV-III Cone and Plate Viscometer, Brookfield Engineering Laboratories, Inc., Stoughton, MA 02072.
23. C. Miao, S. N. Shafirir, J. C. Lambropoulos, J. Mici, and S. D. Jacobs, *Appl. Opt.* **48**, 2585 (2009).
24. Zygo NewView™ 100 White Light Optical Profiler, areal over 0.25 mm × 0.35 mm with a 20× Mirau objective, no filter, Zygo Corporation, Middlefield, CT 06455.
25. Zygo NewView™ 100 White Light Optical Profiler, 1× Mirau objective, 0.8× zoom, no filter, Zygo Corporation, Middlefield, CT 06455.
26. W. I. Kordonski and S. D. Jacobs, *Int. J. Mod. Phys. B* **10**, 2837 (1996).
27. “Preparing a Stable Aqueous Suspension from a Powder,” Colloidal Dynamics, Ponte Vedra Beach, FL 32082.
28. A. B. Shorey, “Mechanisms of Material Removal in Magnetorheological Finishing (MRF) of Glass,” Ph.D. thesis, University of Rochester, 2000.
29. S. D. Jacobs, F. Yang, E. M. Fess, J. B. Feingold, B. E. Gillman, W. I. Kordonski, H. Edwards, and D. Golini, in *Optical Manufacturing and Testing II*, edited by H. P. Stahl (SPIE, Bellingham, WA, 1997), Vol. 3134, pp. 258–269.